

# 1 **Assimilation of Terrestrial Water Storage from** 2 **GRACE in a Snow-Dominated Basin**

B. A. Forman<sup>1,2</sup>, R. H. Reichle<sup>1</sup>, and M. Rodell<sup>3</sup>

3 **Index Terms:** 1847 (Modeling); 1855 (Remote sensing); 1863 (Snow); 3315 (Data Assimila-  
4 tion); GRACE;

---

B. A. Forman, Global Modeling and Assimilation Office, NASA Goddard Space Flight Center,  
Code 610.1, Greenbelt, MD 20771, USA. (Barton.A.Forman@nasa.gov)

R. H. Reichle, Global Modeling and Assimilation Office, NASA Goddard Space Flight Center,  
Code 610.1, Greenbelt, MD 20771, USA.

M. Rodell, Hydrological Sciences Branch, NASA Goddard Space Flight Center, Code 614.3,  
Greenbelt, MD 20771, USA.

<sup>1</sup>Global Modeling and Assimilation Office,  
NASA Goddard Space Flight Center

<sup>2</sup>Oak Ridge Associated Universities

<sup>3</sup>Hydrological Sciences Branch, NASA  
Goddard Space Flight Center

5 **Abstract.** Terrestrial water storage (TWS) information derived from  
6 Gravity Recovery and Climate Experiment (GRACE) measurements is as-  
7 similated into a land surface model over the Mackenzie River basin lo-  
8 cated in northwest Canada. Assimilation is conducted using an ensemble  
9 Kalman smoother (EnKS). Model estimates with and without assimilation  
10 are compared against independent observational data sets of snow water  
11 equivalent (SWE) and runoff. For SWE, modest improvements in mean  
12 difference (MD) and root mean squared difference (RMSD) are achieved as  
13 a result of the assimilation. No significant differences in temporal correla-  
14 tions of SWE resulted. Runoff statistics of MD remain relatively unchanged  
15 while RMSD statistics, in general, are improved in most of the sub-basins.  
16 Temporal correlations are degraded within the most upstream sub-basin,  
17 but are, in general, improved at the downstream locations, which are more  
18 representative of an integrated basin response. GRACE assimilation using  
19 an EnKS offers improvements in hydrologic state/flux estimation, though  
20 comparisons with observed runoff would be enhanced by the use of river  
21 routing and lake storage routines within the prognostic land surface model.  
22 Further, GRACE hydrology products would benefit from the inclusion of  
23 better constrained models of post-glacial rebound, which significantly af-  
24 fects ~~estimation~~GRACE estimates of interannual hydrologic variability in the  
25 Mackenzie River basin.

## 1. Introduction

26 Snow is an important component of the hydrologic cycle that accounts for a large  
27 fraction of the available freshwater resources in many parts of the northern hemisphere  
28 [*Barnett et al.*, 2005]. Accurate estimation of snow mass, or snow water equivalent (SWE),  
29 across space and time using point-scale, ground-based techniques is a difficult task. There-  
30 fore, in an effort to better quantify this potential freshwater supply, many researchers have  
31 turned to remote sensing estimates derived from space-based instrumentation used in con-  
32 junction with land surface models.

33 Despite recent popularity in the utilization of passive microwave and visible spectrum  
34 imagery for the purpose of snow pack estimation (e.g., *Andreadis and Lettenmaier* [2006];  
35 *Durand and Margulis* [2006]; *Dong et al.* [2007]; *Su et al.* [2008]), satellite-derived measure-  
36 ment techniques possess significant limitations. Passive microwave estimates, for example,  
37 are prone to large errors for snow packs that are either wet, deep ( $> 1$  m), or contain ice  
38 and/or depth hoar layers [*Clifford*, 2010]. Similarly, visible imagery often provides little  
39 information outside of the initial accumulation and final ablation periods of the snow  
40 season [*Clark et al.*, 2006].

41 An alternative to passive microwave and visible spectrum-based SWE estimation is the  
42 use of gravimetry. Gravimetric techniques focus on the measurement of gravitational  
43 anomalies associated with the accumulation (or loss) of mass near the Earth's surface.  
44 In the context of snow, changes in the Earth's gravitational field are associated with the  
45 accumulation of snow during the snow season and the subsequent ablation and runoff of  
46 the snow mass during the melt season. Gravimetry is capable of capturing snow mass

47 throughout the accumulation season, including peak accumulation when SWE information  
48 is most valuable to water resource managers. Unfortunately, the drawback of space-based  
49 gravimetry is its coarse spatial ( $\sim$ hundreds of km) and temporal ( $\sim$ monthly) resolution  
50 that limits its applicability for smaller domains. When satellite gravimetric measurements  
51 are combined with a land surface model as part of a data assimilation (DA) framework,  
52 however, there is the potential to effectively downscale gravimetric estimates in time and  
53 space while simultaneously providing useful information content when passive microwave  
54 and visible spectrum measurements cannot.

## 2. Background

55 One such satellite gravimetry mission is the Gravity Recovery and Climate Experiment  
56 (GRACE). GRACE provides approximately monthly estimates of variations in terrestrial  
57 water storage (TWS), which includes snow, ice, surface water, soil moisture, and ground-  
58 water. The mission is a major step towards understanding regional TWS dynamics [*Tang*  
59 *et al.*, 2010] and offers significant insight into regional- and continental-scale hydrologic  
60 processes [*Syed et al.*, 2009; *Rodell et al.*, 2009].

61 Relatively few studies have been conducted that utilize GRACE measurements within a  
62 DA framework. The first study by *Zaitchik et al.* [2008] assimilated GRACE information  
63 into a land surface model of the Mississippi River basin. When compared against in-  
64 situ groundwater observations, *Zaitchik et al.* [2008] found reduced errors and increased  
65 temporal correlations as a result of the assimilation. Further, the results suggested the  
66 potential to downscale the coarse-scale GRACE measurements via use of a relatively fine-  
67 scale land surface model. However, due to the fact that snow contributes little to TWS in

68 the Mississippi River basin, there was limited opportunity to study the impact of GRACE  
69 data assimilation on snow pack characterization.

70 More recently, *Su et al.* [2010] studied the impact of GRACE data assimilation on TWS  
71 estimates in North America for the express purpose of improved snow pack estimation.  
72 They found that GRACE assimilation improved SWE estimation in many of the North  
73 American basins where snowfall is a significant contributor to the hydrologic cycle. How-  
74 ever, *Su et al.* [2010] also found that many issues remain to be addressed, including: 1)  
75 the cause of model degradation in some high-latitude basins as a result of GRACE assim-  
76 ilation, 2) the impact of GRACE observational error on DA results, and 3) the impact of  
77 GRACE assimilation on components of TWS other than snow.

78 This study expands on the work by *Zaitchik et al.* [2008] and *Su et al.* [2010] via  
79 extended examination of GRACE DA performance within a snow-dominated hydrologic  
80 basin. Namely, additional verification activities using independent, ground-based data  
81 sets are explored, a number of different GRACE products are tested during assimilation,  
82 the impact of GRACE measurement error on DA results is investigated, an analysis of DA  
83 innovation sequences is included, and a longer period of record is utilized, which allows  
84 for a better assessment of inter-annual variability.

85 The following sections introduce the methods used in the assimilation framework (sec-  
86 tion 3), [highlight the study domain \(section 4\)](#), discuss the GRACE measurements and  
87 forward model used during the assimilation (section 5), highlight the independent data  
88 sets used for ~~model-verification~~[validation](#) (section 6), present ~~model~~[assimilation](#) results (section  
89 7), and conclude with summarized findings and implications (section 8).

### 3. Data Assimilation Framework

90 A DA framework is an effective means of merging model estimates with measurements  
91 that often yields an improved estimate beyond that of the model or measurements alone  
92 [*McLaughlin*, 2002]. Not only does DA provide a conditioned estimate that accounts  
93 for both model and measurement uncertainty, but it offers the potential to effectively  
94 downscale the measurements in space and time via utilization of the finer-scale information  
95 associated with the prognostic model formulation, its parameters, and its forcing data  
96 [*Reichle et al.*, 2001; *Zaitchik et al.*, 2008].

97 Selection of the most appropriate DA system depends on feasibility, robustness, and  
98 computational efficiency. In that regard, we choose to employ an Ensemble Kalman  
99 Smoother (EnKS) in part because of its ability to handle non-linear models coupled  
100 with its flexible, modular structure [*Dunne and Entekhabi*, 2006] as well as the ability  
101 to leverage *Zaitchik et al.* [2008] as a precursor study. In general, an EnKS has two ba-  
102 sic components: 1) a physically-based, forward model to propagate the model states as  
103 an ensemble in order to provide background error covariances, and 2) an update scheme  
104 that combines the model states and the satellite measurements in a way that accounts  
105 for their respective uncertainties. The work conducted in this current study adapts the  
106 EnKS presented in *Zaitchik et al.* [2008] for a snow-dominated basin thereby contributing  
107 to the methodological development of GRACE DA (see section 5.3). The EnKS is first  
108 introduced below whereas the assimilated measurements and forward model are discussed  
109 in section 5.

### 3.1. Ensemble Kalman Smoother

110 The prior (unconditioned) estimate of the model states,  $\mathbf{x}_\tau^{i-}$ , is derived from a prog-  
 111 nostic land surface model. This is illustrated in the left-hand side (i.e., Step 1) of Figure 1.  
 112 The nonlinear model,  $\mathcal{F}_t(\cdot)$ , propagates the posterior (conditioned) model states,  $\mathbf{x}_{\tau-1}^{i+}$ ,  
 113 forward in time,  $t$ , from  ~~$t-1$~~  to one month to the next (i.e., from  $\tau-1$  to  $\tau$ ) using an  
 114 ensemble of  $N$  realizations with prescribed model errors  $\mathbf{w}_t^i$  as

$$\mathbf{x}_\tau^{i-} = \mathcal{F}_t(\mathbf{x}_{\tau-1}^{i+}, \mathbf{w}_t^i) \text{ for } i \in N. \quad (1)$$

115 We adopt the convention where bold lowercase symbols denote vectors, bold uppercase  
 116 symbols denote matrices, non-bold symbols denote scalars, and calligraphic symbols rep-  
 117 resent operators. Uncertainties in the model are defined by the model error term,  $\mathbf{w}_t^i$  with  
 118 covariance  $\mathbf{Q}_t$ . In the ensemble framework, model errors are represented by perturbations  
 119 that are applied to model states and forcings (section 5).

120 Next, the prior model states are updated using the observations available for the time  
 121 period of interest  $\tau \in [t_o, t_f]$  (where  $t_o$  and  $t_f$  are the beginning and end of the assimilation  
 122 ~~period~~window, i.e., first and last day of the month in this application). This is illustrated  
 123 in the right-hand side (i.e., Step 2) of Figure 1. The following linear update equation is  
 124 employed as

$$\mathbf{x}_\tau^{i+} = \mathbf{x}_\tau^{i-} + \mathbf{K}_\tau [\mathbf{y}_\tau + \mathbf{v}^i - \mathbf{H}\mathbf{x}_\tau^{i-}], \quad (2)$$

125 where  $\mathbf{K}_\tau$  is the Kalman gain matrix,  $\mathbf{y}_\tau$  is the measurement vector, and  $\mathbf{H}$  is the pre-  
 126 dicted measurement model that linearly maps the model states into measurement space.  
 127 Random perturbations,  $\mathbf{v}^i$ , representing measurement error are added to the measurement

128 vector [*Burgers et al.*, 1998]. The Kalman gain,  $\mathbf{K}_\tau$ , is a weighted average between the  
 129 uncertainty of the prior states and the measurements such that

$$\mathbf{K}_\tau = \mathbf{P}_\tau^- \mathbf{H}_\tau^T (\mathbf{H}_\tau \mathbf{P}_\tau^- \mathbf{H}_\tau^T + \mathbf{R})^{-1}, \quad (3)$$

130 where  $\mathbf{P}_\tau^-$  is the background error covariance computed from  $\mathbf{x}_\tau^{i-}$  for  $i \in [1N]$ , and  $\mathbf{R}$  is the  
 131 measurement error covariance. The analysis increments,  $\mathbf{x}_\tau^+ - \mathbf{x}_\tau^-$ , are applied evenly over  
 132 each day of the month as illustrated in Step 2 of Figure 1. The update procedure ignores  
 133 non-Gaussian characteristics and relies only on the first two moments of the distribution.  
 134 In practice, however, it may only be feasible to accurately compute the first and second  
 135 moments of the system state [*Khare et al.*, 2008]. Additional details regarding the EnKS  
 136 update procedure applied in Equation (2) are found in Figure 5 of *Zaitchik et al.* [2008]  
 137 as well as in section 5.3 further below.

#### 4. Study Domain

138 The study domain used here is the Mackenzie River basin (MRB) located in north-  
 139 western Canada (Figure 2) and consists of 4 individual sub-basins. Sub-basin delineation  
 140 was based on topographic control and adhered to the topology of the river network. Each  
 141 sub-basin was extracted from the original GRACE product in order to produce sub-basin-  
 142 averaged TWS estimates. The smallest sub-basin is 280,000 km<sup>2</sup>, which is larger than the  
 143 minimum area of roughly 150,000 km<sup>2</sup> that can be resolved by GRACE at mid-latitudes  
 144 [*Rowlands et al.*, 2005; *Swenson et al.*, 2006]. Additional details regarding the GRACE  
 145 measurements and measurement preprocessing activities are found in section 5.1 and sec-  
 146 tion 5.2, respectively.



147 As a whole, MRB is  $\sim 1.8 \times 10^6$  km<sup>2</sup> in drainage area ( $\sim 1.6 \times 10^6$  km<sup>2</sup> for land areas only;  
148 see Table 1) with the main branch of the Mackenzie River running from the highlands in  
149 the southwestern corner of the domain northward toward the Arctic Ocean. The snow  
150 classification scheme of *Sturm et al.* [2010] suggests MRB snow type is dominated by taiga-  
151 type snow with smaller areas of tundra- and alpine-type snow found in the northwest and  
152 southern regions, respectively (see Figure 2b).

## 5. Assimilated Measurements and Forward Model

### 5.1. GRACE Measurements Background

153 Several different GRACE hydrology products were investigated in this study. TWS  
154 anomalies from 1) the Space Geodesy Research Group (GRGS) product [*Bruinsma et al.*,  
155 2010; *Horwath et al.*, 2011], 2) the Tellus product available from the NASA Jet Propul-  
156 sion Laboratory (Tellus) [*Wahr et al.*, 2004; *Swenson and Wahr*, 2006], and 3) the mass  
157 concentration product generated at the NASA Goddard Space Flight Center (MasCon)  
158 [*Rowlands et al.*, 2005, 2010]. Each product utilizes the same Level 1 range-rate measure-  
159 ments from GRACE, but is processed in a different manner in order to yield mass change  
160 estimates in terms of equivalent water thickness.

161 Each product is available as gridded TWS anomalies (i.e., deviations from the temporal  
162 mean at each location). The GRGS and Tellus products are provided on a  $\sim 1^\circ \times 1^\circ$   
163 grid whereas the MasCon product is provided on a  $\sim 4^\circ \times 4^\circ$  grid. Each product was  
164 subsequently converted into sub-basin-averaged total TWS values by adding the location-  
165 specific, ~~temporal-mean~~ long-term average TWS from the land surface model. More infor-  
166 mation on GRACE measurement preprocessing is provided in section 5.2 and the land  
167 surface model is provided in section 5.3.

## 5.2. GRACE Measurement Preprocessing

168 Conversion of the GRACE TWS anomalies into sub-basin-averaged TWS estimates  
169 that are compatible with modeled TWS values begins with generating a single-replicate  
170 of the forward model for the period 1 September 2002 to 1 September 2009. No model  
171 errors are prescribed in this simulation unlike that shown in Equation (1). ~~Temporally~~Long-  
172 term (i.e., 2002-2009) averaged, sub-basin-averaged estimates of TWS derived from the  
173 forward model are subsequently added to the sub-basin-averaged monthly GRACE TWS  
174 anomalies, which yields monthly estimates of TWS for each modeled sub-basin that are  
175 eventually assimilated using Equation (2). Additional details on the utilization of the  
176 GRACE measurements in Equation (2) are found in *Zaitchik et al.* [2008].

177 One notable aspect of GRACE preprocessing is the consideration of a secular trend  
178 associated with post-glacial rebound (PGR). The Tellus product accounts for PGR using  
179 the methods of *Paulson et al.* [2007]. However, the GRGS and MasCon products do not  
180 account for PGR. Therefore, model output from *Paulson et al.* [2007] is applied here to  
181 the GRGS and MasCon products in a similar manner as done for the Tellus product.  
182 Preliminary DA results suggest PGR is overestimated by the model of *Paulson et al.*  
183 [2007] in both the Slave and Peace+Athabasca sub-basins, but this cannot be verified  
184 as the exact amount of PGR in these regions is unknown. Unfortunately, PGR models  
185 are difficult to validate due to a lack of independent data, thus the errors are not well  
186 quantified. Therefore, in an effort to better understand the impacts of PGR estimates  
187 on GRACE DA performance within the MRB, two different versions of each GRACE  
188 product were used in the DA experiments: 1) PGR correction applied using *Paulson et*  
189 *al.* [2007] and 2) PGR correction *not* applied (i.e., PGR correction was removed from the

190 Tellus product). These two approaches effectively bound the extent of PGR impacts on  
191 GRACE DA performance.

192 Finally, one requirement for optimal data assimilation is an accurate representation  
193 of measurement error. Given the multiple sources of error present within the GRACE  
194 measurements [*Bruinsma et al.*, 2010; *Horwath et al.*, 2011; *Rowlands et al.*, 2005; *Swenson*  
195 *and Wahr*, 2006; *Wahr et al.*, 2006], this task is not trivial. GRACE TWS errors arise  
196 from a combination of measurement errors, processing errors, and errors in the geophysical  
197 models used to de-alias the GRACE measurements [*Wahr et al.*, 2004]. The error estimates  
198 used in this study ~~generally agree with~~ are based on those of *Swenson and Wahr* [2006] and  
199 *Swenson* [In Prep.], and are comparable to those used in *Zaitchik et al.* [2008]. Even  
200 though the spatially-distributed error estimates provided in *Swenson* [In Prep.] are only  
201 for the Tellus product, we believe they are fairly representative of the measurement error  
202 in all the GRACE products since each product utilizes the same Level 1 range-rate mea-  
203 surements. The time-invariant GRACE measurement error used in this study is less than  
204 that used in *Zaitchik et al.* [2008] due to the increased number of satellite overpasses near  
205 the poles. The measurement error covariance for each sub-basin of interest is provided  
206 in Table 1. The impact of measurement error covariance on DA performance is further  
207 discussed in section 7.4.

### 5.3. Catchment Land Surface Model

208 The prognostic model used in this application is the Catchment Land Surface Model  
209 (Catchment) developed by *Koster et al.* [2000]. Catchment employs a catchment deficit  
210 prognostic variable rather than the more commonly-used soil water content variable to  
211 estimate subsurface water storage, and explicitly models sub-grid scale soil moisture vari-

212 ability and its effect on hydrological processes such as runoff and evaporation. Further, the  
213 inclusion of a three-layer snow model [*Stieglitz et al.*, 2001] provides additional capability  
214 in the estimation of terrestrial water storage in areas where snow is a significant contrib-  
215 utor to the hydrologic cycle. These attributes create a unique capability for Catchment  
216 in the assimilation of terrestrial water storage data assimilation.

217 The predicted measurement model,  $\mathbf{H}$ , (see Equation (2)) maps the Catchment model  
218 states into the GRACE measurement space.  $\mathbf{H}$  not only spatially aggregates the model  
219 states into the 4 sub-basins as described in section 5.1, but it also integrates the model  
220 states to yield a vertically integrated estimate of TWS. Catchment-based estimates of  
221 TWS include changes in the unconfined water table, root-zone soil moisture, surface  
222 soil moisture, SWE, and canopy interception. A schematic of Catchment-derived TWS is  
223 shown in Figure 3. Catchment-derived TWS was computed in a similar manner as done in  
224 *Zaitchik et al.* [2008] except with the additional consideration of canopy interception. Even  
225 though lake water storage can be a significant storage component of TWS, Catchment  
226 does not account for mass changes within surface water impoundments.

227 The ~~Goddard Earth Observing System Version 5.2.0 (GEOS-5)~~ Modern Era Retrospective-Analysis for  
228 Research and Application (MERRA) product [*Rienecker et al.*, 2011], ~~of which Catchment is a~~  
229 ~~part,~~ was used to force the land surface model. MERRA is provided at an hourly temporal  
230 resolution and a  $1/2^\circ \times 2/3^\circ$  (latitude/longitude) spatial resolution. An alternative forcing  
231 data set by *Reichle et al.* [2011] was investigated for use, which is the same as MERRA  
232 except that the precipitation estimates have been corrected towards estimates from the  
233 Global Precipitation Climatology Project (GPCP) [*Huffman et al.*, 1997] ~~through rescaling of~~  
234 ~~the MERRA precipitation such that the total amount of precipitation matched that found in the original GPCP.~~ No

235 significant difference in the performance of the DA experiments was found between the two  
236 forcing data sets. Therefore, only the results utilizing the MERRA forcing are presented  
237 here.

238 Perturbations to specified model states and forcings were prescribed in order to ade-  
239 quately represent model error. Both multiplicative and additive perturbations were uti-  
240 lized as listed in Table 2. Model state perturbations were applied every 20 minutes (i.e., at  
241 each model time step) whereas model forcing perturbations were applied every 60 minutes  
242 (i.e., at each forcing time step). Temporal correlations were imposed using a first-order  
243 auto-regressive model (AR(1)) within the perturbed fields as discussed in *Reichle et al.*  
244 [2008]. Following the work of *Reichle and Koster* [2003], a horizontal error correlation  
245 length of  $2.0^\circ$  was applied. The root zone soil moisture excess prognostic variable was not  
246 perturbed to avoid the introduction of unwanted bias in the subsurface. Cross-correlations  
247 between perturbations were included in an analogous manner as conducted in *Reichle et*  
248 *al.* [2007].

249 To better manage perturbations made to the Catchment ensemble, a number of mod-  
250 ifications were made to the DA framework from that originally used in *Zaitchik et al.*  
251 [2008]. Perturbations applied to the 3 snow layers were only applied to SWE and not to  
252 snow depth or snow heat content. Perturbed snow depth was subsequently recomputed  
253 as the perturbed SWE divided by the unperturbed snow density. Snow heat content was  
254 also recomputed such that the perturbed SWE yielded the same snow pack temperature  
255 as the unperturbed SWE. This was done to ensure physical consistency within the snow  
256 pack associated with the prescribed SWE perturbations. In addition, perturbations to  
257 the catchment deficit (subsurface) were modified based on the presence of snow in con-

258 junction with frozen soil conditions. More specifically, if snow is present and the surface  
259 ( $\sim 5$  cm) soil temperature is below freezing, perturbations are applied to the SWE states  
260 only; if the surface soil temperature is at or above freezing, perturbations are applied to  
261 the SWE states as well as the catchment deficit. Conversely, if snow is absent and the  
262 surface soil temperature is below freezing, perturbations applied to the catchment deficit  
263 state were scaled by a factor  $< 1$  in order to mimic the attenuated soil moisture dynamics  
264 associated with reduced soil permeability; if the surface soil temperature is at or above  
265 freezing, perturbations were applied normally to the catchment deficit. Collectively, the  
266 changes better maintain physical consistency within the snow pack while better simulating  
267 an attenuated soil moisture response when frozen soil conditions persist.

268 Model spin-up and initialization consisted of a two-step approach. The first step in-  
269 volved a repeated, one-year (i.e., May 2001 to May 2002) cycle of a single replicate without  
270 model perturbations for ten years to yield a reasonable estimate of TWS. The second step  
271 involved running the model as an open-loop (OL) ensemble from May 2002 to September  
272 2002 in order to yield a reasonable estimate of cross-correlations between different model  
273 states as well as to produce an adequate amount of uncertainty (spread) within the OL  
274 ensemble. From September 2002 to September 2009, the model was run in either OL  
275 mode or with GRACE DA enabled. Finally, an ensemble size of 16 was used based on  
276 the convergence of the TWS standard deviation of the prior ensemble. Ensemble sizes  
277 greater than 16 showed no significant change in ensemble standard deviation, hence it was  
278 determined that 16 replicates was sufficiently large.

## 6. Validation Approach

279 A variety of observational data sets were used to evaluate the GRACE DA output.  
280 However, due to the observation sparsity within the MRB, particularly in the northern  
281 regions, not all pertinent model states could be verified. Most notable amongst the obser-  
282 vational data gap is a lack of groundwater and soil moisture measurements. Despite the  
283 lack of some observational types, a series of modeled and measured estimates are avail-  
284 able that provide a reasonable assessment of the MRB hydrologic response as a function  
285 of space and time.

### 6.1. CMC Daily Snow Analysis Product

286 Snow observations were based on the Canadian Meteorological Centre (CMC) daily  
287 snow depth product [*Brasnett, 1999; Brown and Brasnett, 2010*] obtained via ftp server  
288 at `sidads.colorado.edu` . The CMC product yields snow depth estimates throughout  
289 the northern hemisphere at a horizontal resolution of  $\sim 24$  km for the period of March  
290 1998 to the present, and is often considered the best available snow product for evaluating  
291 model output [*Su et al., 2010*]. It is based on optimal interpolation of in situ daily snow  
292 depth observations and aviation reports with a first-guess field generated from a simple  
293 snow model driven by analyzed temperatures and forecast precipitation from the Canadian  
294 forecast model [*Brasnett, 1999*]. SWE estimates were derived from the CMC daily snow  
295 depth estimate in conjunction with the climatological snow density parameterization of  
296 *Sturm et al. [2010]* as a function of snow depth, day of year, and snow class (Figure 2b).

### 6.2. INAC Snow Surveys

297 An additional set of ground-based observations was made available by the Indian and  
298 Northern Affairs Council (INAC). This observational dataset consists of snow surveys at

299 42 different locations, predominantly within the Slave Basin (Figure 2b). Each survey  
300 consisted of snow depth and snow water equivalent measurements at  $\sim 10$  different points  
301 that were then averaged together to yield a single survey estimate at each of the 42 different  
302 survey locations. In general, surveys were conducted annually when the snow pack reached  
303 peak accumulation. Therefore, these ground-based observations are only available once  
304 per year and only within a small portion of the MRB. Between the CMC measurement  
305 product and the INAC observational dataset, however, a reasonable comparison of SWE  
306 estimates may be conducted over the entire MRB domain throughout the course of the  
307 snow season with particular emphasis placed on peak accumulation.

### 6.3. GRDC Runoff Observations

308 Runoff estimates were provided by The Global Runoff Data Center (GRDC) via [http://www.bafg.de/GRDC/EN/Home/homepage\\_\\_node.html](http://www.bafg.de/GRDC/EN/Home/homepage__node.html). GRDC estimates are available  
309 at hundreds of locations within the MRB at a daily timescale. However, only a handful  
310 of stations were selected based on a minimum upland drainage area of  $\geq 250,000$  km<sup>2</sup>  
311 and a minimum of six (6) years of measurements (Figure 2a). Daily estimates were  
312 subsequently aggregated to a monthly timescale for comparison against the DA results  
313 utilizing monthly GRACE observations. Table 3 lists the stations used in this study  
314 along with the approximate sub-basin aggregation (in terms of integrated upland area)  
315 in accordance with the sub-basins shown in Figure 2a. GRDC discharge estimates in  
316 the MRB are, in general, based on measurements of river stage height, which were then  
317 converted into volumetric flux using assumptions of river cross-sectional area and flow  
318 velocity. During the winter time when ice floes are common in the MRB, river discharge  
319 measurement error likely increases.  
320



#### 6.4. Validation Metrics

Using the independent, ground-based observations described above, a number of validation metrics were computed. Mean difference (MD) was computed as  $MD = \frac{1}{T} \sum_{t=1}^T (M_t - O_t)$  where  $M_t$  is the modeled ensemble mean and  $O_t$  is the ground-based observation, respectively, at time  $t$  and where  $T$  is the total number of time steps. Similarly, root mean squared difference (RMSD) was computed as  $RMSD = \frac{1}{T} \sqrt{\sum_{t=1}^T (M_t - O_t)^2}$ . Finally, the anomaly correlation coefficient (R) was computed by first determining the climatological seasonal cycle over the course of the simulation period, then the anomaly time series is computed by subtracting the climatological seasonal cycle from the original time series, and finally the anomaly R is computed as the correlation coefficient between the modeled ensemble mean anomalies and the corresponding anomalies of the ground-based observations. For all 3 metrics, the modeled values are obtained from either the open-loop (OL) or data assimilation (DA) simulations. In addition, only times and locations with values  $M_t > 0$  or  $O_t > 0$  were used in the computation. That is, coincident zeros were excluded (e.g. omitting summertime values when no snow is present in both the model and observations).

Statistical significance of R is determined using the Hotelling-Williams Test, which investigates the equality of two dependent correlations [Steiger, 1980]. In this study, the dependent correlations are between: 1) the ground-based observations and the OL results ( $R_{12}$ ), and 2) the ground-based observations and the DA results ( $R_{13}$ ). It begins with the hypothesis that the two dependent correlations are equal (i.e.,  $H_o : R_{12} = R_{13}$ ). Next, a t-statistic is computed as

$$t_{N-3} \sim (R_{12} - R_{13}) \sqrt{\frac{(N-1)(1+R_{23})}{2\frac{N-1}{N-3}|R| + \bar{R}^2(1-R_{23})^3}}, \quad (4)$$

342 where  $N$  is the approximate number of degrees of freedom,  $\bar{R} = \frac{R_{12}+R_{13}}{2}$ ,  $R_{23}$  is the  
 343 correlation between the OL and DA results, and  $|R| = 1 - R_{12}^2 - R_{13}^2 - R_{23}^2 + 2R_{12}R_{13}R_{23}$ .  
 344 If the computed t-statistic is greater than the corresponding Student t-statistic for a given  
 345  $N$  at a given confidence level, then one can reject the null hypothesis,  $H_o$ , and in turn  
 346 say that the computed correlation coefficients are statistically different. It is important to  
 347 note that the t-statistic computed here is only an approximation and likely overestimates  
 348 the value because of the presence of serial error correlations, which imply that the actual  
 349 number of degrees of freedom is less than the number of data points.

## 7. Results and Discussion

### 7.1. Terrestrial Water Storage (TWS)

350 Comparison of model results begins with a comparison against the assimilated GRACE  
 351 TWS measurements used during the conditioning phase. Theory predicts that if informa-  
 352 tion transfer from the GRACE observations into the model estimates takes place during  
 353 conditioning, then a better agreement between the conditioned estimates and the GRACE  
 354 observations should occur. If not, the lack of change is either due to a near-zero covari-  
 355 ance structure in  $\mathbf{K}$  or is due to close agreement between the GRACE TWS and the  
 356 model-predicted TWS.

357 Figure 4 shows the ensemble OL and DA simulations relative to the GRGS (without  
 358 PGR correction) GRACE TWS observations for the 4 assimilated sub-basins along with  
 359 the MRB as a whole. The dark gray and light gray regions represent the range of the OL  
 360 and DA ensembles, respectively. The GRACE observations are shown as solid, black dots

361 with the error bars representing the time-invariant standard deviation of the observation  
362 error. The thick dashed and solid lines represent the ensemble means for the OL and DA  
363 ensembles, respectively.

364 In general, there is good agreement between the OL ensemble mean and the GRACE  
365 measurements with the exception of the Slave basin during 2002-2004. When DA is  
366 enabled, the ensemble mean moves toward the GRACE observations as a result of con-  
367 ditioning. The presence of positive, non-zero covariances in  $\mathbf{K}$  coupled with differences  
368 between the GRACE observations and the model-based TWS estimates allows for a signif-  
369 icant correction in the DA ensemble toward the GRACE observations. However, it should  
370 also be noted that significant differences exist between the model estimates (OL and DA)  
371 and the GRACE observations near the annual minimum of TWS. This is in part due to  
372 a bias in the variability between the OL model and the observations. That is, the Catch-  
373 ment model has a tendency to “dry out” beyond what the GRACE measurements would  
374 suggest. As is discussed in more detail in section 7.3 and 8, a lack of hydraulic routing  
375 and lake storage routines in Catchment leads to a more rapid hydrologic response, which  
376 results in a more variable (i.e., larger dynamic range) estimate of TWS. Assimilation of  
377 the GRACE measurements serves to constrain some of this variability. In addition, when  
378 the snow melts and subsequently runs off, the model-derived background error variance  
379 is smaller (due to a lack of snow and snow errors) than the prescribed measurement er-  
380 ror variance, which ultimately leads to a significant reduction in the Kalman gain (see  
381 Equation (4)) and hence a ~~relatively-small~~smaller update towards the GRACE measurements.

382 After conditioning, another notable feature is that the ensemble spread is significantly  
383 reduced between the OL and DA simulations. This is indicative of the DA procedure

384 having an impact on the model-derived ensemble and suggests increased confidence in the  
385 TWS estimates via assimilation. Collectively, these findings compose a useful sanity check  
386 on the efficacy of the assimilation framework and lends some credibility to its ability to  
387 model TWS in a snow-dominated basin.

## 7.2. Snow Water Equivalent (SWE)

### 388 7.2.1. Comparison to CMC Product

389 Monthly-averaged CMC values of SWE for each of the four sub-basins as well as the  
390 entire MRB are compared against the OL and DA simulations. As discussed in section 5.2,  
391 multiple versions of each GRACE product were generated that include PGR corrections  
392 as well as exclude PGR corrections using the model of *Paulson et al.* [2007]. For brevity  
393 only the GRGS product is discussed herein as it is representative of the other GRACE  
394 products and because it yields the most complete timeseries (i.e., fewest monthly gaps) for  
395 the study simulation period. Further, only the results for the GRGS product excluding  
396 PGR corrections are shown in Figure 5. The sensitivity to the PGR corrections will be  
397 discussed later.

398 Differences in Figure 5 between the OL and DA simulations are apparent, most no-  
399 tably the reduction in ensemble ~~spread (uncertainty)~~standard deviation (spread) associated  
400 with GRACE assimilation. In general, the conditioning procedure moves the DA en-  
401 semble mean closer to the CMC estimates relative to the OL simulation. This is more  
402 apparent in the Liard basin where the snowfall accumulation is greatest, particularly in  
403 2005-2007 and 2009 when the model has a tendency to overestimate SWE. Changes are  
404 less apparent in the other sub-basins because less snow is present, hence the changes are  
405 much smaller in magnitude, and because in general, the OL does a reasonable job of esti-

406 mating SWE. This is further discussed in section 7.5 where it is shown that the updates  
407 to SWE are near-zero during much of the accumulation phase, hence differences in OL  
408 and DA SWE are relatively small.

409 Figure 6 shows statistics of MD, RMSD, and anomaly R for each of the sub-basins.  
410 Metrics are shown for the open loop (white), and for assimilation of GRGS GRACE TWS  
411 without (light gray) and with (dark gray) PGR correction. In terms of MD and RMSD  
412 without PGR correction, the greatest improvement is witnessed in the Liard basin. MD  
413 relative to the CMC product is reduced through assimilation by  $\sim 30\%$  (MD=13.2 mm  
414 for OL and MD=9.3 mm for DA) with a  $>15\%$  reduction in RMSD (RMSD=24 for OL  
415 and RMSD=19.6 for DA). The other sub-basins, including the MRB as a whole, contain  
416 less snow and receive a much smaller amount of correction compared to the Liard basin.  
417 In general, the other sub-basins receive a small reduction in MD with little or no change  
418 to RMSD. Changes in MD and RMSD of SWE are essentially the same no matter which  
419 GRACE product is assimilated and no matter whether PGR correction is or is not applied  
420 (results not shown).

421 Unlike MD and RMSD, changes to anomaly R are typically degraded as a result of  
422 the assimilation. When excluding PGR correction, the differences are not statistically  
423 significant at the 5% level based on the Hotelling-Williams Test, but there are apparent  
424 reductions in the ability to capture the inter-annual variability of SWE when invoking the  
425 DA procedure. These results suggest the DA simulations do a reasonable job of estimating  
426 the amount of SWE in each basin but that the timing of the accumulation/ablation  
427 phases are slightly degraded when incorporating information from GRACE. When PGR  
428 correction is applied to the GRACE observations, the anomaly R degradation becomes

429 much more pronounced, particularly in the Slave basin where PGR is most prominent in  
430 the model of *Paulson et al.* [2007] ( $R=0.70$  for DA without PGR correction and  $R=0.64$   
431 for DA with PGR correction). More specifically, assimilation of the GRGS product with  
432 PGR correction yields the lowest anomaly  $R$  values among basins in both the Slave sub-  
433 basin and the MRB as a whole with values that are statistically different from the OL  
434 results via the Hotelling-Williams test.

### 435 7.2.2. Comparison to INAC Surveys

436 On average both the OL and DA simulations underestimate SWE when compared  
437 against the INAC ground-based observations with  $MD=-28$  mm for OL and  $MD=-33$   
438 mm for DA estimates (Table 4). Each comparison was conducted by first comparing all  
439 of the surveys at a given location in space against the model output collocated in time.  
440 Then, the MD and RMSD was computed across time and subsequently presented in Table  
441 4. The assimilation of GRACE data typically removes snow mass near peak accumula-  
442 tion thereby further increasing the negative bias. The INAC observations are in direct  
443 contrast to the CMC product results, which suggest a positive bias in the OL and DA  
444 results. However, given that the CMC product is conditioned on snow depth observations  
445 collected in open areas such as airports that are subject to wind-blown snow redistribu-  
446 tion, there is a potential to introduce a negative bias into the CMC estimates (relative to  
447 the truth). Snow at the stations used in the CMC optimal interpolation routine tends to  
448 be shallower and melt earlier than in surrounding terrain [*Brown et al.*, 2003]. Hence, the  
449 disparity between the CMC product and the INAC observations within the Slave basin  
450 can be partly explained by the CMC negative bias (relative to the truth) as well as by

451 the differences in the sampling domain between point-scale observations and the  $\sim 24$ -km  
452 pixel resolution of the CMC product.

### 7.3. Runoff

453 Comparison against GRDC runoff measurements were conducted in a similar manner  
454 as with the CMC SWE estimates. However, rather than comparing by sub-basin, runoff  
455 estimates are compared against individual gauging stations. Table 3 lists the upland area  
456 and approximate sub-basin integration for each station of interest. Results are displayed  
457 in Figure 7. One notices many distinct features. Namely, all simulations (OL or DA)  
458 suffer from a significant negative bias relative to the runoff observations. This is mostly  
459 due to insufficient baseflow runoff within the model for all but the smallest of sub-basins.  
460 This is clearly demonstrated in Figure 7 at the downstream observation locations dur-  
461 ing the winter when melt flux and overland flow are near-zero because the surface water  
462 (e.g. SWE) is restrained in solid phase. Hence, the baseflow component is the dominant  
463 contributor to winter runoff. Since the observed runoff at the downstream locations is  
464 considerably larger than the modeled runoff, it is reasonable to assume that the model  
465 generates an insufficient amount of baseflow at these locations during the winter season  
466 when overland flow is minimized. One also notices an overestimation of annual peak flow,  
467 particularly during the spring freshet. This is partly due to a lack of runoff routing and  
468 lake storage routines, which contributes to a more rapid runoff response within the model.  
469 No discernible difference between the OL and DA ensemble means is witnessed in Figure  
470 7 as the DA line effectively overlaps the OL line. However, a small ( $\sim 5$ -10%) reduction  
471 in ensemble standard deviation (spread) is witnessed in most sub-basins as a result of the  
472 assimilation procedure.

473 Figure 8 shows the corresponding computed statistics of MD, RMSD, and anomaly  
474 R at a monthly timescale at each of the gauging stations. In general, MD is slightly  
475 more negative as a result of assimilation, but to a lesser degree when PGR correction  
476 is excluded (light gray) relative to the inclusion of PGR correction (dark gray). The  
477 decrease in negative MD results from the removal of SWE during peak accumulation,  
478 which results in less runoff production during ablation. The removal of SWE is essentially  
479 counter-balanced by an increase in subsurface storage (further discussed in section 7.5),  
480 but does not translate into any significant increase in baseflow production or infiltration  
481 excess runoff, hence the slightly more negative MD. RMSD, in general, is reduced or  
482 remains unchanged in all of the sub-basins and is effectively the same between the different  
483 GRACE products (results not shown).

484 The greatest discord between the different assimilation experiments is found in the  
485 anomaly R values. The GRGS product without PGR correction, in general, yielded the  
486 best results. However, 2 out of 6 station locations are degraded as a result of GRACE  
487 assimilation relative to the OL results. Station number 4 (S+L+P+A in Figure 8c)  
488 undergoes a statistically significant level of improvement ( $R=0.25$  for OL and  $R=0.30$   
489 for DA without PGR correction), but at the cost of statistically significant degradations  
490 at the first station (L in Figure 8c;  $R=0.71$  for OL and  $R=0.64$  for DA without PGR  
491 correction) and fifth station (S+L+P+A+B in Figure 8c;  $R=0.50$  for OL and  $R=0.46$   
492 for DA without PGR correction). When PGR correction is included, more stations are  
493 degraded than are improved with most station degradations being significant at the 5%  
494 level. These results, in conjunction with the SWE results, suggest assimilation of the



495 GRGS product excluding PGR correction yields the greatest amount of improvement  
496 (and least amount of degradation) in terms of inter-annual variability.

497 Finally, in order to investigate the potential impact of a river routing scheme, an analysis  
498 was conducted in which runoff estimates (OL or DA) were computed using a simple,  
499 fixed-lag smoother. For a given month, the fixed-lag smoother computed the runoff as  
500 the average of the given month and the preceding  $n$  months ~~preceding~~. This effectively  
501 delays the hydrologic runoff response in a manner analogous to that of a runoff routing  
502 scheme. Based on the anomaly R and RMSD statistics between the GRDC observations  
503 and the runoff computed from the fixed-lag smoother (results not shown), the greatest  
504 improvements typically occur with a temporal lag of 1-2 months. However, the general  
505 conclusions with or without application of the fixed-lag smoother remain the same in that  
506 the runoff response with GRACE assimilation is improved, albeit by a small amount.  
507 Therefore, even though the results displayed in Figure 8c do not account for hydraulic  
508 routing, the results serve as a good proxy of the impact of GRACE assimilation on runoff  
509 estimation.

#### 7.4. Normalized Innovation Sequence

510 A filter innovation is the difference between the ensemble mean observation and model  
511 forecast,  $\mathbf{y}_t - \mathbf{H}\mathbf{x}_t^-$ , at a given time,  $t$ . Investigation of filter innovations is a useful tool  
512 for assessing whether or not measurement (Table 1) and model (Table 2) error parameters  
513 have been appropriately selected. If a model is linear and all errors are Gaussian, then the  
514 normalized innovations,  $NI$ , should appear similar in form to white noise (i.e., zero mean,  
515 unit variance, and temporally uncorrelated). Even though the application used here is a  
516 smoother rather than a filter and the forward model is non-linear, the investigation of the

517 normalized innovations can provide useful information as to the performance of the DA  
 518 procedure.

519 The normalized innovation may be written as

$$NI_t = \frac{\mathbf{y}_t - \mathbf{H}\mathbf{x}_t^-}{\sqrt{\mathbf{H}\mathbf{P}_t^-\mathbf{H}^T + \mathbf{R}}}, \quad (5)$$

520 where the numerator represents the difference between the assimilated measurement and  
 521 the predicted measurement, and the denominator represents a combination of the back-  
 522 ground error covariance and the measurement error covariance. Normalized innovations  
 523 are collected as a function of time and then the mean is computed as  $\overline{NI} = \frac{1}{T} \sum_{t=1}^T NI_t$   
 524 while the standard deviation computed as  $\sigma_{NI} = \sqrt{\frac{1}{T} \sum_{t=1}^T (NI_t - \overline{NI})^2}$ .

525 Figure 9 plots the mean versus the standard deviation of the normalized innovations  
 526 for each of the four (4) sub-basins using the GRGS product excluding PGR correction.  
 527 The different colors represent different amounts of measurement error standard deviation  
 528 used during the DA experiments relative to the nominal values listed in Table 1. The  
 529 most striking feature is that all of the mean innovations are negative regardless of the  
 530 sub-basin or the measurement error. This suggests the DA procedure attempts to correct  
 531 a systematic bias where the model contains too much water relative to the GRACE  
 532 observations during certain times of the year. This can be seen via inspection of Figure  
 533 4e where the individual sub-basin GRACE updates effectively remove mass most years at  
 534 peak accumulation, particularly after January 2005. During the ablation and runoff phase,  
 535 GRACE DA attempts to add mass in the subsurface, but the amount of mass added is, in  
 536 general, less than the amount of SWE removed. Hence, the result is a posterior ensemble

537 with less TWS. This behavior is further discussed in the following section via inspection  
538 of the analysis increments.

539 The second feature of note in Figure 9 is the wide range in  $\sigma_{NI}$  resulting from changes  
540 to the measurement error standard deviation. As expected, an increase in measurement  
541 error causes an increase in the denominator of Equation (5), which causes a corresponding  
542 reduction in the spread (or standard deviation) of the normalized innovation sequence.  
543 If the design of  $\mathbf{HP}_t^- \mathbf{H}^T$  is assumed reasonable, Figure 9 suggests that  $2\times$  the nominal  
544 measurement error standard deviation of Table 1 is too large. A large measurement error  
545 variance (relative to the background error variance) results in a small value of the gain  
546  $\mathbf{K}$  (Equation (3)), which leads to only minimal assimilation updates. Conversely, a value  
547 of  $0.5\times$  the nominal measurement error standard deviation is too small, which causes  
548 the assimilation to overly “trust” the measurement quality and effectively make too large  
549 of an update toward the GRACE measurements. Based on  $\sigma_{NI}$ , application of  $1.0\times$  to  
550  $1.5\times$  the estimated measurement error appears reasonable and is similar to the GRACE  
551 measurement errors used in *Zaitchik et al.* [2008] and *Su et al.* [2010].

## 7.5. Analysis Increments

552 Investigation of the analysis increments (i.e., difference between  $\mathbf{x}_t^+$  and  $\mathbf{x}_t^-$ ) can provide  
553 valuable insight into the behavior of the assimilation procedure. It enables one to track  
554 mass within the relevant TWS components in order to see how much and at what time  
555 mass is being added to or removed from the system. Figure 10 shows the analysis incre-  
556 ments from the assimilation of the GRGS product excluding PGR correction. The thin,  
557 solid line shows the increments made to the subsurface TWS component as the negative  
558 of the catchment deficit prognostic variable. Assimilation updates were not applied to the

559 surface soil excess or root zone soil excess states. However, this is inconsequential as the  
560 efficacy with which Catchment redistributes water in the subsurface is overwhelmingly  
561 dominated by the catchment deficit variable [Zaitchik *et al.*, 2008]. Averaged over time  
562 and space the increments are positive for a total of 12.5 mm, which means assimilation  
563 results in increasing the amount of water in the subsurface. This is most evident during  
564 the spring and summer. The thick, dashed line shows the increments for SWE summed  
565 across the three individual SWE layers. Averaged over time and space SWE is removed  
566 during the accumulation phase with a small amount added back during the ablation and  
567 runoff phase for a total SWE increment of -45.1 mm. Collectively, the analysis increments  
568 to the catchment deficit and SWE serve to reduce mass during snow accumulation and  
569 then increase the mass during ablation and runoff. These two phenomena essentially con-  
570 strain the amplitude of the modeled TWS dynamics such that better agreement with the  
571 GRACE observations is achieved.

## 8. Conclusions

572 GRACE-derived estimates of TWS were assimilated into a land surface model for the  
573 purpose of improved snow pack characterization in northwestern Canada. It was shown  
574 that the conditioning procedure, in general, could reduce MD and RMSD in the SWE esti-  
575 mates (prior versus posterior) when compared against the CMC snow product. However,  
576 anomaly R values were typically degraded as a result of the assimilation. Even though  
577 the anomaly R differences were not statistically significant at the 5% level, they suggest  
578 some degree of reduced skill at simulating inter-annual variability when using the DA  
579 procedure. A comparison of model results against GRDC runoff observations suggested  
580 relatively little change to runoff MD and RMSD statistics. Anomaly R values for runoff,

581 however, were improved at several locations and remain essentially unchanged at the basin  
582 outlet. Improvements to anomaly R values for runoff are mostly attributable to a more  
583 delayed runoff response with assimilation.

584 These results are encouraging, but it is important to highlight shortcomings and discuss  
585 potential improvements that could be made in future developments. For example, the  
586 land surface model used in this study does not contain a river routing scheme. Runoff is  
587 effectively routed to the outlet instantaneously. However, given the size and extent of the  
588 MRB, runoff residence times near the basin outlet can be conservatively estimated to be  
589 on the order of a couple of months. The improvements to runoff anomaly R values are  
590 generally associated with a delayed runoff response that effectively retains water within  
591 the basin for a longer period of time. That is, the assimilation acts to correct some of the  
592 limitations in the model physics that could likely be addressed via inclusion of a runoff  
593 routing routine. Similarly, the land surface model does not contain a lake storage routine.  
594 Changes in lake storage can be a significant contributor to TWS and can also be an  
595 important factor in attenuating hydrologic runoff response at the basin outlet. Analogous  
596 to a runoff routing routine, inclusion of a lake level storage routine could likely improve  
597 runoff timing relative to the GRDC observations. Development and testing of runoff  
598 routing and lake storage routines are beyond the scope of this current study, but would  
599 be worthwhile addressing in future work.

600 In addition, another limitation of this study is a lack of subsurface observations (i.e., soil  
601 moisture and groundwater) to evaluate model results. Updates to the catchment deficit  
602 prognostic variable can only be discussed in a qualitative sense without a valid dataset  
603 to make quantitative comparisons. Unfortunately, soil moisture and groundwater level

604 measurements are not readily available in hydrologic basins located in the high latitudes  
605 thereby making such a comparison difficult if not impossible. The lack of subsurface  
606 observations severely limits the conclusions that can be made about the ability of the  
607 assimilation to effectively disaggregate TWS into snow, soil moisture, and groundwater  
608 components.

609 Despite these shortcomings, the GRACE DA procedure did improve MD and RMSD  
610 statistics of SWE in the MRB as well as improved some runoff estimates in terms of inter-  
611 annual variability. These preliminary findings are encouraging and suggest the potential  
612 for further improvements via merger with passive microwave and visible spectrum remote  
613 sensing products to further downscale the GRACE observations in time and space while  
614 simultaneously disaggregating the GRACE observations into individual, vertical compo-  
615 nents of TWS. Finally, additional improvements could be achieved through refining the  
616 GRACE measurement error model, investigating the effects of different horizontal error  
617 correlation lengths within the land surface model forcings, determining a more optimal  
618 GRACE measurement scale, utilizing a more optimal GRACE averaging kernel, and bet-  
619 ter constraining of PGR model estimates used during GRACE preprocessing.

620 **Acknowledgments.** Funding provided by the NASA Postdoctoral Program Fellow-  
621 ship (Contract NNH06CC03B). Additional thanks go to Ross Brown for answers to our  
622 questions regarding the CMC snow analysis product; Derek Faria for access to the INAC  
623 snow surveys; Ulrich Looser for access to the GRDC database; John Wahr, Sean Swen-  
624 son, and Felix Landerer for discussions on PGR; and Bailing Li for many constructive  
625 comments.

## References

- 626 K.M. Andreadis and D.P. Lettenmaier. Assimilating remotely sensed snow observations  
627 into a macroscale hydrology model. *Adv. Water Resour.*, 29:872–886, 2006.
- 628 T.P. Barnett, J.C. Adam, and D.P. Lettenmaier. Potential impacts of a warming climate  
629 on water availability in snow-dominated regions. *Nature*, 438:303–309, 2005.
- 630 B. Brasnett. A global analysis of snow depth for numerical weather prediction. *J. Appl.*  
631 *Meteorol.*, 38:726–740, 1999.
- 632 S. Bruinsma, J.-M. Lemoine, R. Biancale, and N. Valès. CNES/GRGS 10-day gravity  
633 field models (release 2) and the evaluation. *Adv. Space Res.*, 45:587–601, 2010.
- 634 R.D. Brown and B. Brasnett. Canadian Meteorological Centre (CMC) daily snow depth  
635 analysis data. Environment Canada, 2010. Boulder, Colorado USA: National Snow and  
636 Ice Data Center. Digital media.
- 637 R.D. Brown, B. Brasnett, and D. Robinson. Gridded North American monthly snow  
638 depth and snow water equivalent for GCM evaluation. *Atmos. Ocean*, 41:1–14, 2003.
- 639 G. Burgers, P.J. van Leeuwen, and G. Evensen. Analysis scheme in the ensemble Kalman  
640 filter. *Mon. Weather Rev.*, 126:1719–1724, 1998.
- 641 M.P. Clark, A.G. Slater, A.P. Barrett, L.E. Hay, G.J. McCabe, B. Rajagopalan, and  
642 G.H. Leavesley. Assimilation of snow covered area information into hydrologic and  
643 land-surface models. *Adv. Water Resour.*, 29:1209–1221, 2006.
- 644 D. Clifford Global estimates of snow water equivalent from passive microwave instruments:  
645 History, challenges, and future developments. *Int. J. Remote Sens.*, 31:3707–3726, 2010.
- 646 J. Dong, J.P. Walker, P.R. Houser, and C. Sun. Scanning multichannel mi-  
647 crowave radiometer snow water equivalent assimilation. *J. Geophys. Res.*,

- 648 112:doi:10.1029/2006JD007209, 2007.
- 649 M.T. Durand and S.A. Margulis. Feasibility test of multi-frequency radiometric data  
650 assimilation to estimate snow water equivalent. *J. Hydrometeorol.*, 7:443–457, 2006.
- 651 S. Dunne and D. Entekhabi. Land surface state and flux estimation using the ensemble  
652 Kalman smoother during the Southern Great Plains 1997 field experiment. *Water*  
653 *Resour. Res.*, 42:doi:10.1029/2005WR004334, 2006.
- 654 M. Horwath, J.-M. Lemoine, R. Biancale, and S. Bourgoigne. Improved GRACE science  
655 results after adjustment of geometric biases in the Level-1B K-band ranging data. *J.*  
656 *Geod.*, 85–23:38, 2011.
- 657 G.J. Huffman, R.F. Adler, P.A. Arkin, A. Chang, R. Ferraro, A. Gruber, J. Janowiak,  
658 A. McNab, B. Rudolf, and U. Schneider. The global precipitation climatology project  
659 (GPCP) combined precipitation dataset. *B. Am. Meteorol. Soc.*, 78:5–20, 1997.
- 660 S.P. Khare, J.L. Anderson, T.J. Hoar, and D. Nychka. An investigation into the applica-  
661 tion of an ensemble Kalman smoother to high-dimensional geophysical systems. *Tellus*,  
662 60A:97–112, 2008.
- 663 R.D. Koster, M.J. Suarez, A. Ducharne, M. Stieglitz, and P. Kumar. A catchment-based  
664 approach to modeling land surface processes in a general circulation model 1. Model  
665 structure. *J. Geophys. Res.*, 105:24809–24822, 2000.
- 666 D.B. McLaughlin. An integrated approach to hydrologic data assimilation: Interpolation,  
667 smoothing, and filtering. *Adv. Water Resour.*, 12:1275–1286, 2002.
- 668 A. Paulson, S. Zhong, and J. Wahr. Inference of mantle viscosity from GRACE and  
669 relative sea level data. *Geophys. J. Int.*, 171:497–508, 2007.



- 670 R.H. Reichle, D. Entekhabi, and D.B. McLaughlin. Downscaling of radio brightness mea-  
671 surements for soil moisture estimation: A four-dimensional variational data assimilation  
672 approach. *Water Resour. Res.*, 37:2353–2364, 2001.
- 673 R.H. Reichle and R.D. Koster. Assessing the impact of horizontal error correlations in  
674 background fields on soil moisture estimation. *J. Hydrometeorol.*, 4:1229–1242, 2003.
- 675 R.H. Reichle, R.D. Koster, P. Liu, S.P.P. Mahanama, E.G. Njoku, and M. Owe. Com-  
676 parison and assimilation of global soil moisture retrievals from the Advanced Mi-  
677 crowave Scanning Radiometer for the Earth Observing System (AMSR-E) and the  
678 Scanning Multichannel Microwave Radiometer (SMMR). *J. Geophys. Res.*, 112:  
679 doi:10.1029/2006JD008033, 2007.
- 680 R.H. Reichle, W.T. Crow, and C.L. Keppenne. An adaptive ensemble Kalman filter for  
681 soil moisture data assimilation. *Water Resour. Res.*, 44: doi:10.1029/2007WR006357,  
682 2008.
- 683 R.H. Reichle, R.D. Koster, G.J.M. De Lannoy, B.A. Forman, Q. Liu, S. Mahanama, and  
684 A. Toure. Assessment and enhancement of MERRA land surface hydrology estimates.  
685 *J. Clim.*, In Press, doi: [10.1175/JCLI-D-10-05033.1](https://doi.org/10.1175/JCLI-D-10-05033.1), 2011.
- 686 M.M. Rienecker, M.J. Suarez, R. Gelaro, R. Todling, J. Bacmeister, E. Liu, M.G.  
687 Bosilovich, S.D. Schubert, L. Takacs, G.-K. Kim, S. Bloom, J. Chen, D. Collins,  
688 A. Conaty, A. da Silva, W. Gu, J. Joiner, R.D. Koster, R. Lucchesi, A. Molod, T. Owens,  
689 S. Pawson, P. Pegion, C.R. Redder, R.H. Reichle, F.R. Robertson, A.G. Ruddick,  
690 M. Sienkiewicz, J. Woolen. MERRA - NASA’s modern-era retrospective analysis for  
691 research and applications. *J. Clim.*, 24:3624–3648, 2011.

- 692 M. Rodell, I. Velicogna, and J.S. Famiglietti. Satellite-based estimates of groundwater  
693 depletion in India. *Nature*, 460:999–1002, 2009.
- 694 D.D. Rowlands, S.B. Luthcke, S.M. Klosko, F.G.R. Lemoine, D.S. Chinn, J.J. Mc-  
695 Carthy, C.M. Cox, and O.B. Anderson. Resolving mass flux at high spatial and  
696 temporal resolution using GRACE intersatellite measurements. *Geophys. Res. Lett.*,  
697 32:doi:10.1029/2004GL021908, 2005.
- 698 D.D. Rowlands, S.B. Luthcke, J.J. McCarthy, S.M. Klosko, D.S. Chinn, F.G. Lemoine,  
699 J.-P. Boy, and T.J. Sabaka. Global mass flux solutions from GRACE: A comparison  
700 of parameter estimation strategies – Mass concentrations versus Stokes coefficients. *J.*  
701 *Geophys. Res.*, 115:doi:10.1029/2009JB006546, 2009.
- 702 J.H. Steiger. Tests for comparing elements of a correlation matrix. *Psychol. Bull.*, 87:245–  
703 251, 1980.
- 704 M. Stieglitz, A. Ducharne, R.D. Koster, and M. Suarez. The impact of detailed snow  
705 physics on the simulation of snow cover and subsurface thermodynamics at continental  
706 scales. *J. Hydrometeorol.*, 2:228–242, 2001.
- 707 M. Sturm, B. Taras, G.E. Liston, C. Derksen, T. Jonas, and J. Lea. Estimating snow water  
708 equivalent using snow depth data and climate classes. *J. Hydrometeorol.*, 11:1380–1394,  
709 2010.
- 710 H. Su, Z.-L. Yang, G.-Y. Niu, and R.E. Dickinson. Enhancing the estimation of  
711 continental-scale snow water equivalent by assimilating MODIS snow cover with the  
712 ensemble Kalman filter. *J. Geophys. Res.*, 113:doi:10.1029/2007JD009232, 2008.
- 713 H. Su, Z.-L. Yang, R.E. Dickinson, C.R. Wilson, and G.-Y. Niu. Multisensor  
714 snow data assimilation at the continental scale: The value of Gravity Recovery

- 715 and Climate Experiment terrestrial water storage information. *J. Geophys. Res.*,  
716 115:doi:10.1029/2009JD013035, 2010.
- 717 S. Swenson, P. J.-F. Yeh, J. Wahr, and J.S. Famiglietti. A comparison of terrestrial water  
718 storage variations from GRACE with in situ measurements from Illinois. *Geophys. Res.*  
719 *Lett.*, 33:doi:10.1029/2006GL026962, 2006.
- 720 S. Swenson and J. Wahr. Post-processing removal of correlated errors in GRACE data.  
721 *Geophys. Res. Lett.*, 33:doi:10.1029/2005GL025285, 2006.
- 722 S. Swenson. Restoring signal loss in GRACE terrestrial water storage estimates. *Geophys.*  
723 *Res. Lett.*, In Preparation, 2011.
- 724 T.H. Syed, J.S. Famiglietti, and D.P. Chambers. GRACE-based estimates of terrestrial  
725 freshwater discharge from basin to continental scales *J. Hydrometeorol.*, 10:22–40, 2009.
- 726 Q. Tang, H. Gao, P. Yeh, T. Oki, F. Su, and D.P. Lettenmaier. Dynamics of terres-  
727 trial water storage change from satellite and surface observations and modeling. *J.*  
728 *Hydrometeorol.*, 11:156–170, 2010.
- 729 J. Wahr, S. Swenson, V. Zlotnicki, and I. Velicogna. Time-variable gravity from GRACE:  
730 first results. *Geophys. Res. Lett.*, 31:doi:10.1029/2004GL019779, 2004.
- 731 J. Wahr, S. Swenson, and I. Velicogna. Accuracy of GRACE Estimates. *Geophys. Res.*  
732 *Lett.*, 33:doi:10.1029/2005GL025305, 2006.
- 733 B.F. Zaitchik, M. Rodell, and R.H. Reichle. Assimilation of GRACE terrestrial water  
734 storage data into a land surface model: Results for the Mississippi river basin. *J.*  
735 *Hydrometeorol.*, 9:doi:10.1175/2007JHM951.1, 2008.

**Table 1.** Sub-basin characteristics for the MRB (land areas only) along with applied GRACE measurement error covariance,  $\mathbf{R}$ .

Sub-basin Name	Land Area [km]	$\mathbf{R}$ [mm <sup>2</sup> ]
Peel+Bear	$4.1 \times 10^5$	$18^2$
Slave	$3.6 \times 10^5$	$16^2$
Liard	$2.8 \times 10^5$	$17^2$
Peace+Athabasca	$5.7 \times 10^5$	$16^2$
Entire Mackenzie	$1.6 \times 10^6$	$17^2$

**Table 2.** Parameters for perturbations to meteorological forcing inputs and model prognostic variables.

Perturbation	Type	Standard Deviation	Units	$\mathbf{L}$ [deg]	AR(1) [day]
Precipitation	M	0.5	-	2	3
Shortwave Radiation	M	0.5	-	2	3
Longwave Radiation	A	50	W m <sup>-2</sup>	2	3
Snow Water Equivalent <sup>a</sup>	M	0.0004	-	2	1
Catchment Deficit	A	0.05	mm	2	1
Surface Soil Excess	A	0.02	mm	2	1

<sup>a</sup>Perturbations made to all three (3) snow layers; M=Multiplicative; A=Additive;  $\mathbf{L}$ =spatial correlation length; AR(1)=first-order auto-regressive temporal correlation

**Table 3.** GRDC runoff measurement characteristics.

Station Number	Station ID	Upland Area [km <sup>2</sup> ]	Sub-basin Aggregation
1	4208271	$2.75 \times 10^5$	Liard
2	4208450	$2.93 \times 10^5$	Peace
3	4208400	$6.06 \times 10^5$	Peace+Athabasca
4	4208005	$1.27 \times 10^6$	Slave+Liard+Peace+Athabasca
5	4208150	$1.57 \times 10^6$	Slave+Liard+Peace+Athabasca+Bear
6	4208025	$1.66 \times 10^6$	Entire Mackenzie

**Table 4.** Statistics for the OL and DA experiments relative to the INAC snow surveys.

Ensemble	MD [mm]	RMSD [mm]
OL	-28	39
DA	-31	41

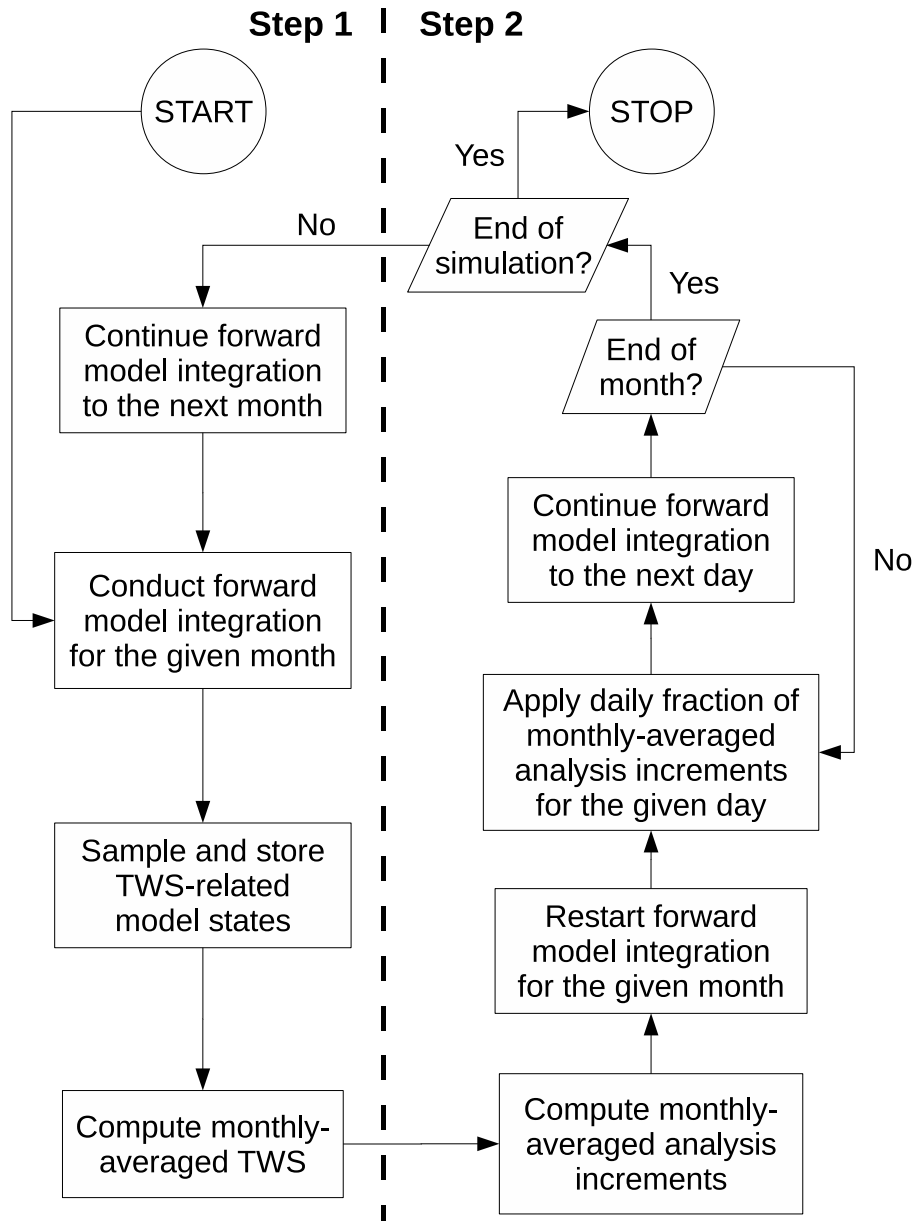
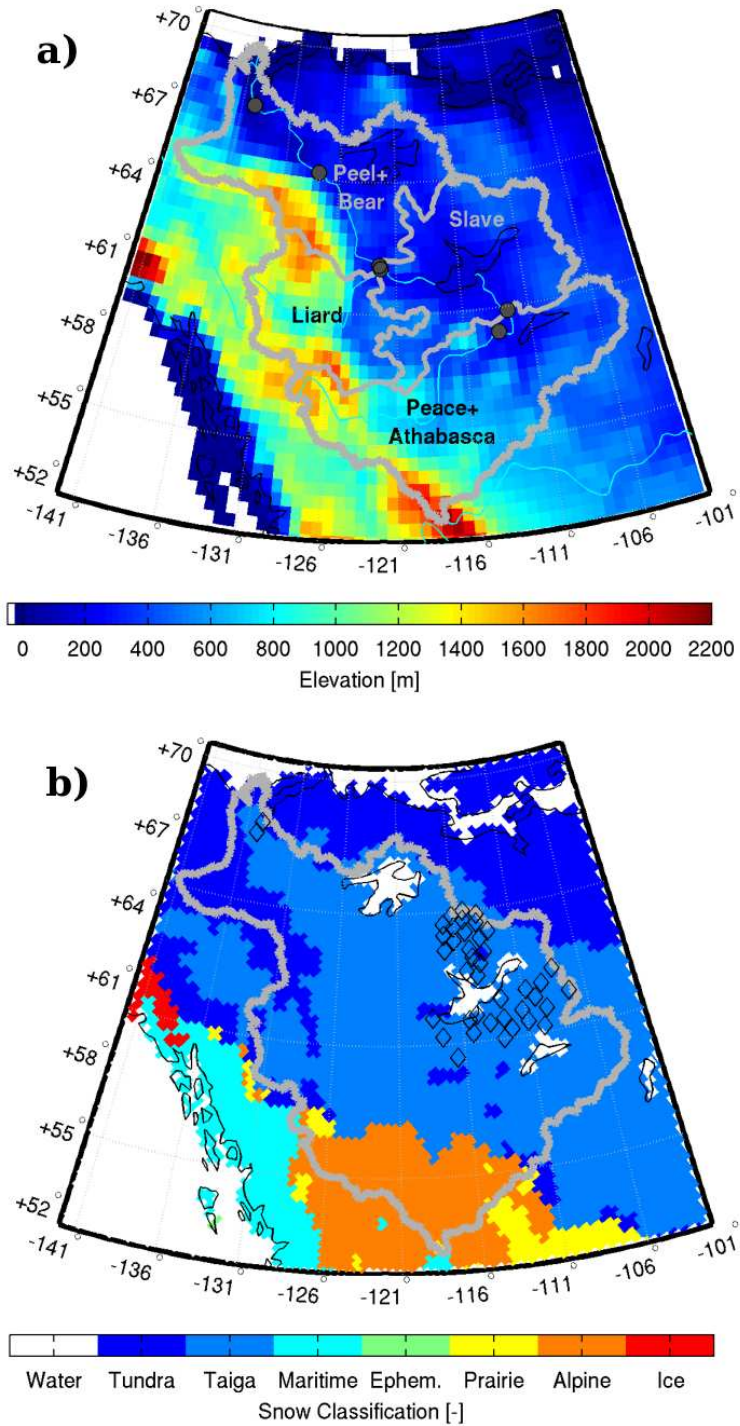
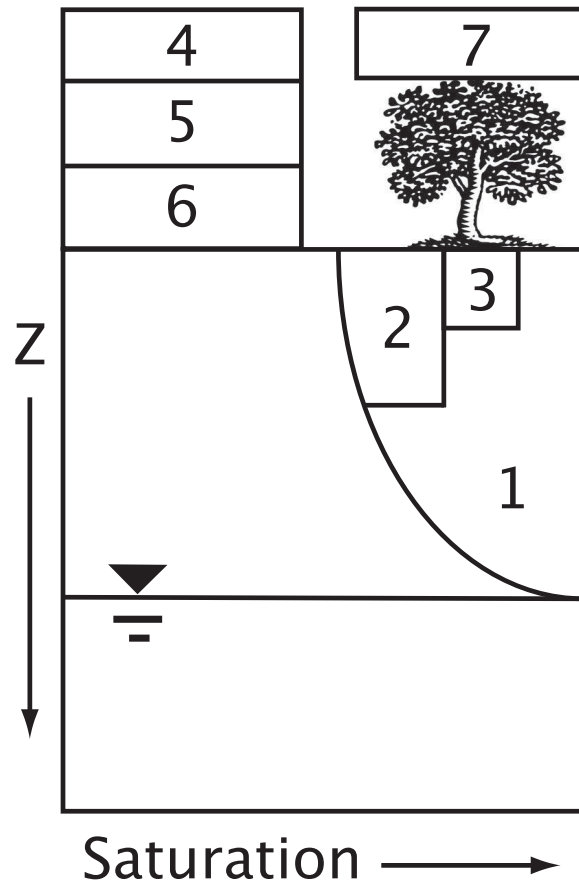


Figure 1. Simplified flowchart of EnKS application.





**Figure 2.** Map of Mackenzie River Basin including a) GEOS-5 topography, sub-basin delineation, and GRDC observation locations (solid dots), and b) *Sturm et al.* [2010] snow type with INAC snow survey locations (hollow diamonds).



**Figure 3.** Conceptual representation of the components of Catchment model terrestrial water storage where 1=catchment deficit, 2=root zone excess, 3=surface soil excess, 4-6=individual snow layers, and 7=canopy interception.

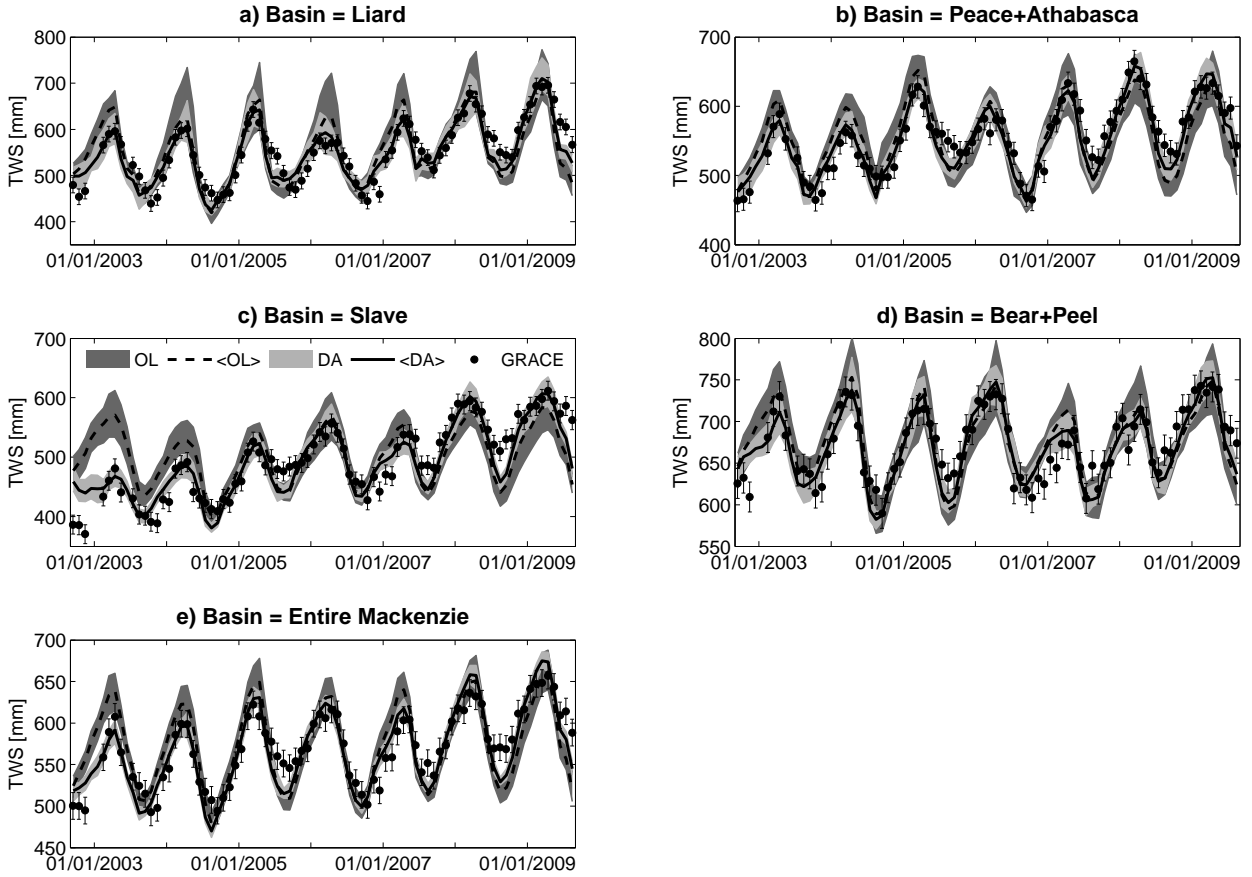


**Figure 4.** TWS estimates for the OL (dark gray), DA (light gray), and GRACE (dots) for the GRGS product without PGR correction. Each line represents the respective ensemble mean whereas the error bars represent the standard deviation of the GRACE observations.

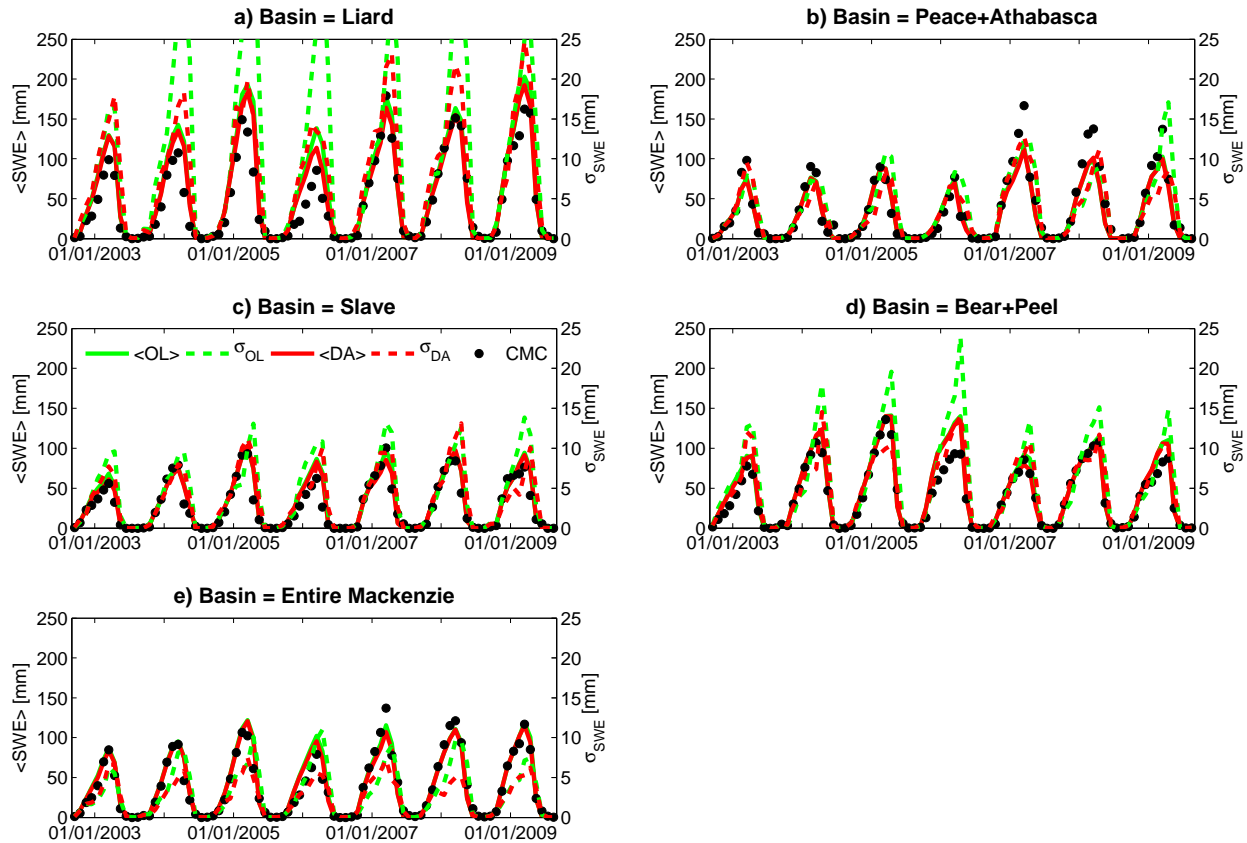


**Figure 5.** SWE estimates from OL (green), DA (red), and CMC (black dots) for the GRGS product without PGR correction. Solid lines represent the ensemble means (left axis) and dashed lines represent the ensemble standard deviations (right axis). CMC SWE estimates were derived from CMC snow depths using *Sturm et al.* [2010] snow densities.

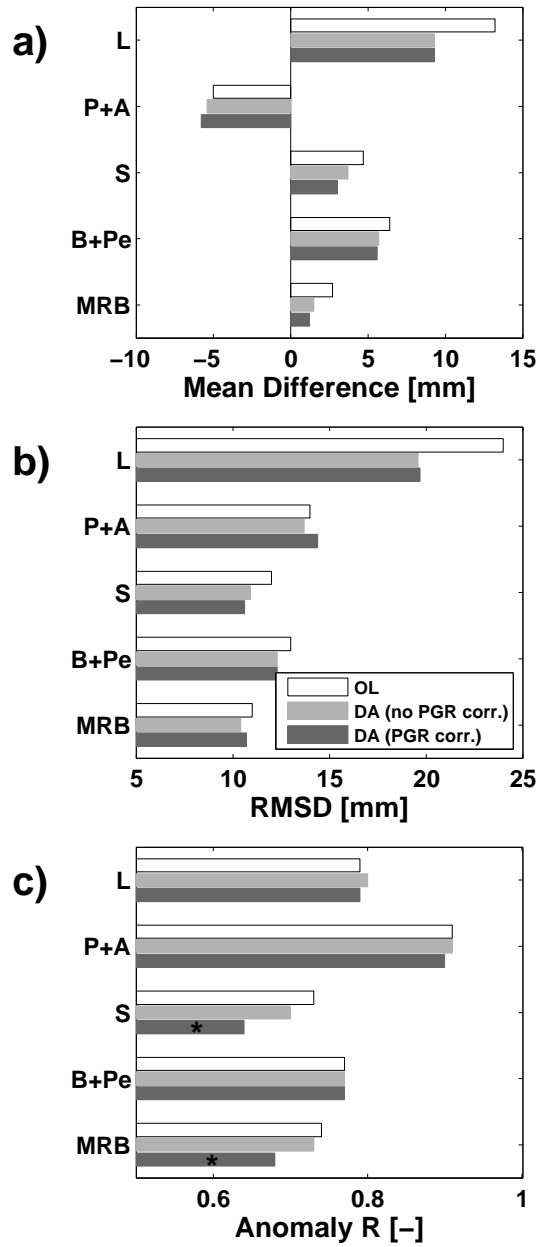


**Figure 6.** SWE statistics of a) MD, b) RMSD, and c) anomaly R for open-loop (white), DA without PGR correction (light gray), and DA with PGR correction (dark gray) results relative to CMC-derived SWE estimates via *Sturm et al.* [2010]. For anomaly R values, asterisks indicate statistically significant differences between the OL and DA.

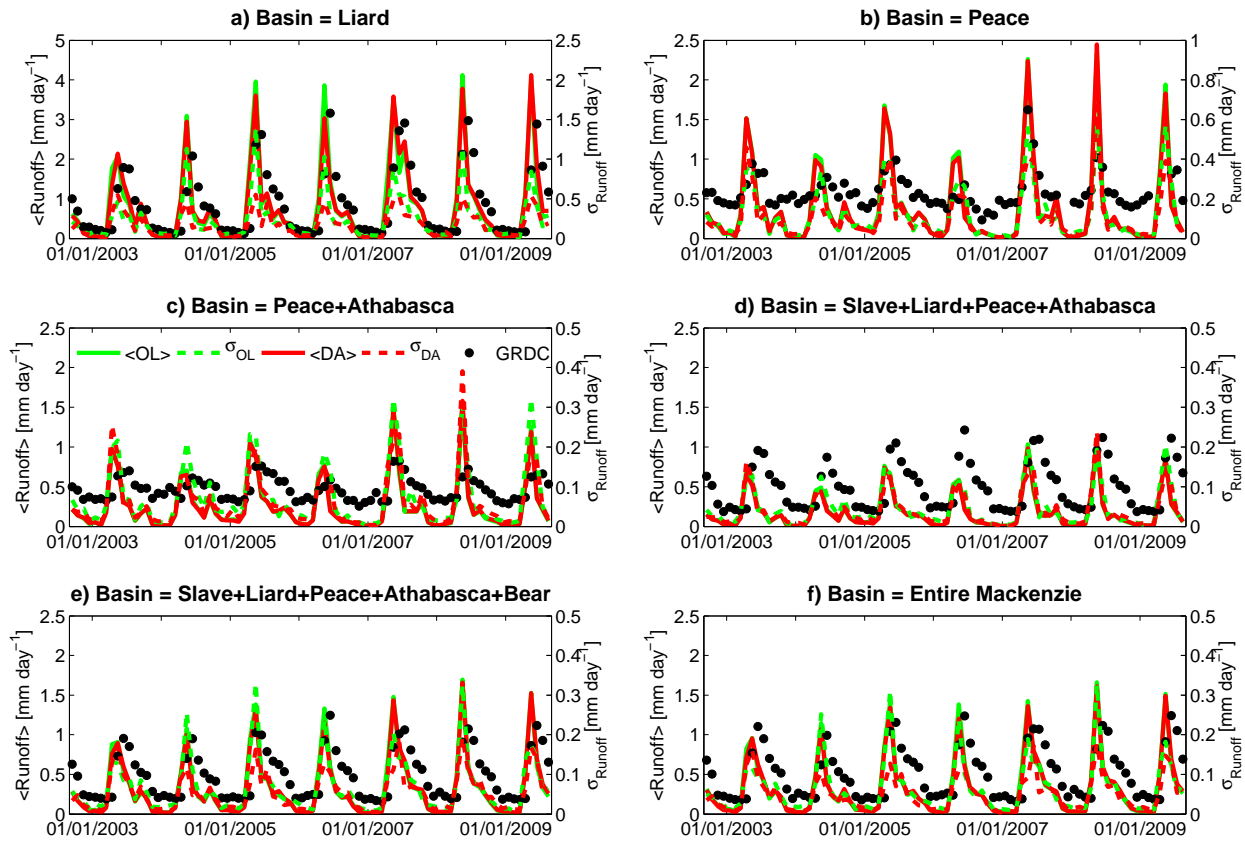


**Figure 7.** Runoff from OL (green), DA (red), and GRDC observations (black dots) at 6 different locations for the GRGS product without PGR correction. Upland drainage area increases from the upper-left subplot through the lower-right subplot (see Table 3 for definitions). Solid lines represent the ensemble means (left axis) and dashed lines represent the ensemble standard deviations (right axis).

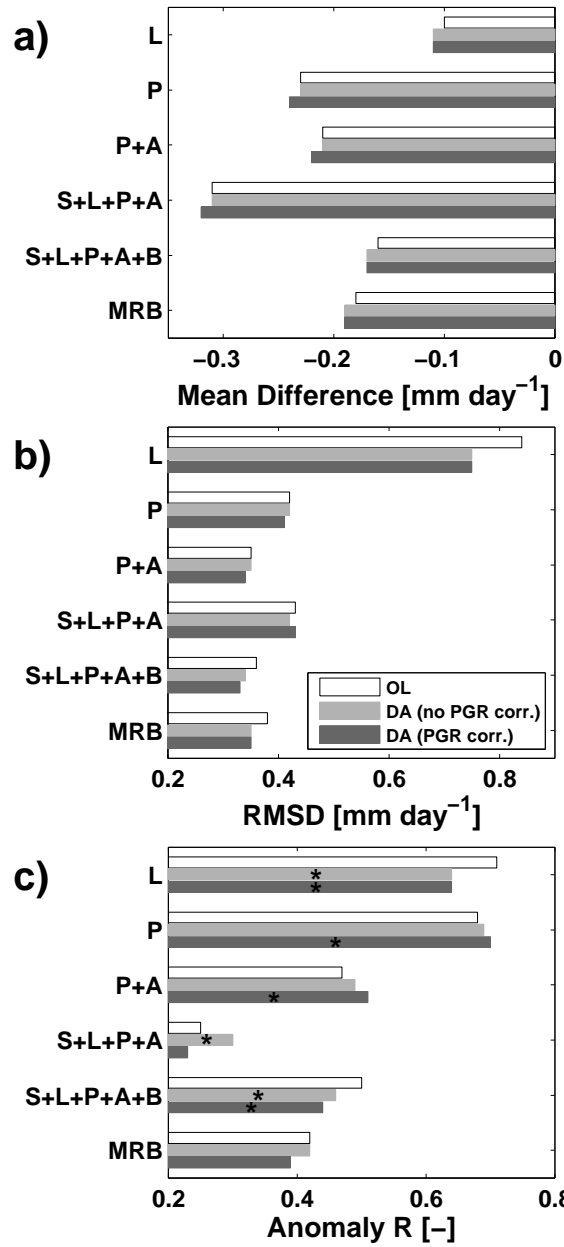


**Figure 8.** Runoff statistics of a) MD, b) RMSD, and c) anomaly R for open-loop (white), DA without PGR correction (light gray), and DA with PGR correction (dark gray) results relative to GRDC runoff estimates for the GRGS product without PGR correction. For anomaly R values, asterisks indicate statistically significant differences between the OL and DA.

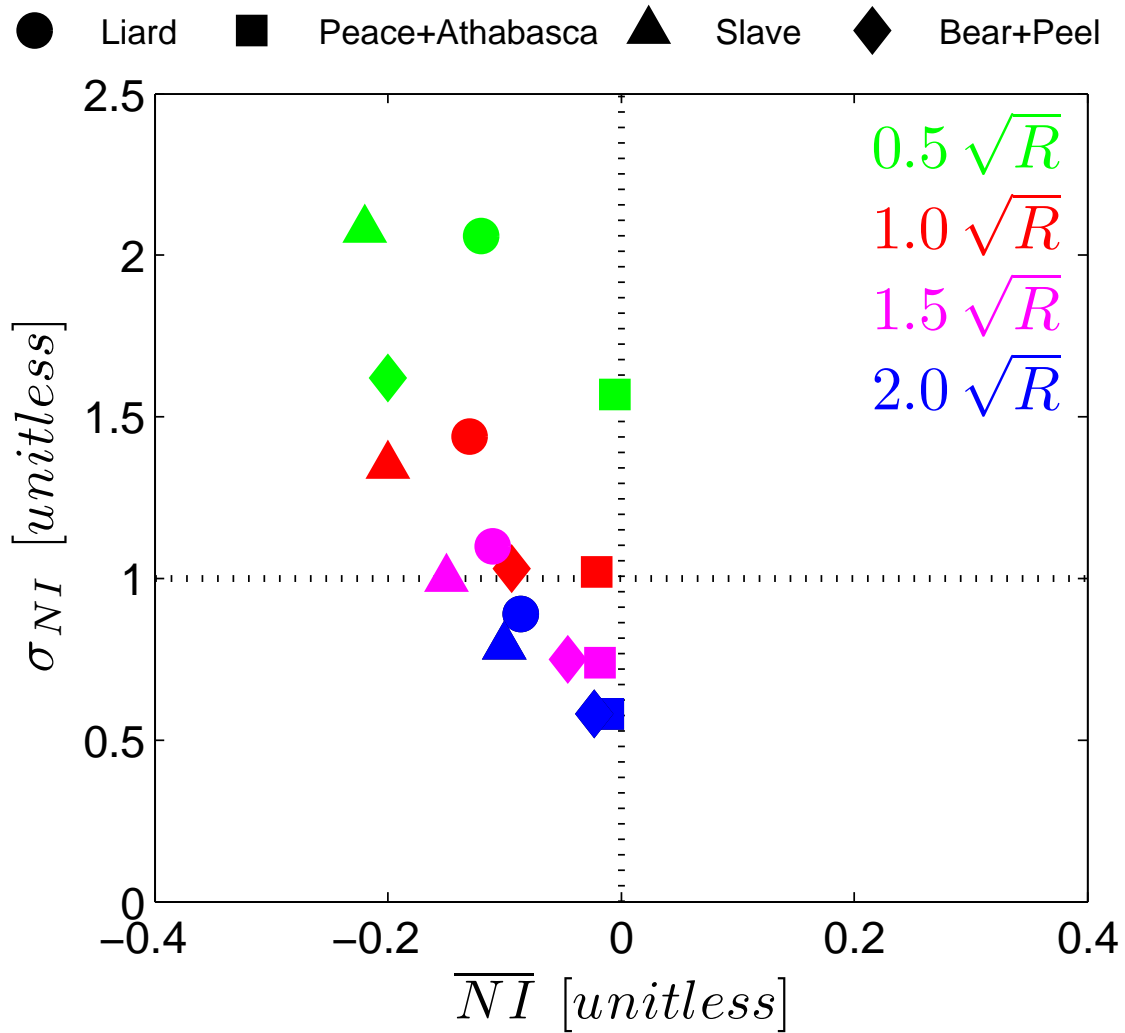


**Figure 9.** Innovation statistics for the GRGS product without PGR correction for the 4 sub-basins shown as different marker shapes. The different marker colors represent varying amounts of GRACE measurement error standard deviation relative to the nominal values shown in Table 1.



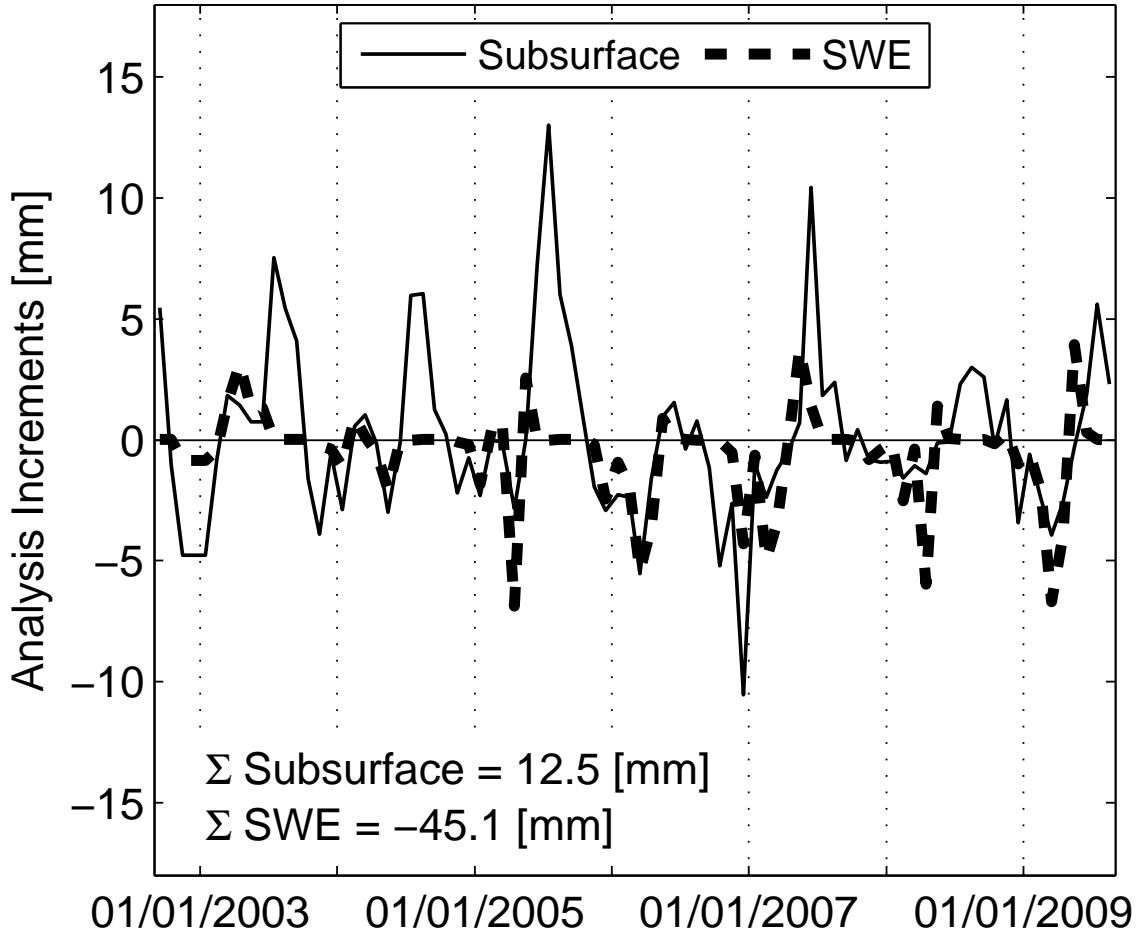


**Figure 10.** Analysis increments for the entire MRB using the GRGS product without PGR correction. The thin, solid line represents the subsurface increments (displayed as the negative of the catchment deficit increments) whereas the thick, dashed line represents the increments from the summation of the three individual SWE layers.